Wind Tunnel Tests of Eight Sailplane Wing-Fuselage Combinations

L.M.M. Boermans
D.C. Terleth

Delft University of Technology
Department of Aerospace Engineering
The Netherlands

Presented at the 18th OSTIV Congress
Hobbs, New Mexico, 1983

INTRODUCTION

When an "optimal" fuselage is added to an "optimal" wing, the performance of the combination may be disappointing due to wing-fuselage interference effects. There is extensive literature on this subject indicating the complexity of the problem, however, publications focussed on sailplane application are scarce. In order to get insight in the flow phenomena and to gather experimental data, also useful in sailplane performance estimation studies, a literature study and a wind tunnel investigation has been performed. The measurements were made in the low-speed, low-turbulence wind tunnel of the Department of Aerospace Engineering at the Delft University of Technology.

The wind tunnel models were provided by DFVLR Braunschweig. They were made and used in a previous wind tunnel experiment by R. Radespiel, Ref. 1. Some results of this study are gratefully quoted.

MODELS

Eight wing-fuselage combinations were obtained by combining three different fuselages with a wing at various positions, Fig. 1.

The basic fuselage, No. 1, is a 1:3 scale fuselage model of the well-known sailplanes ASW-19 and ASW-20. It was chosen because analysis of measured speedpolars indicated relatively low fuselage drag. Fuselages 2 and 3 have the same forebody as fuselage 1, but differ in contraction ratio behind the location of maximum thickness and have a 1/3 thinner tailboom.

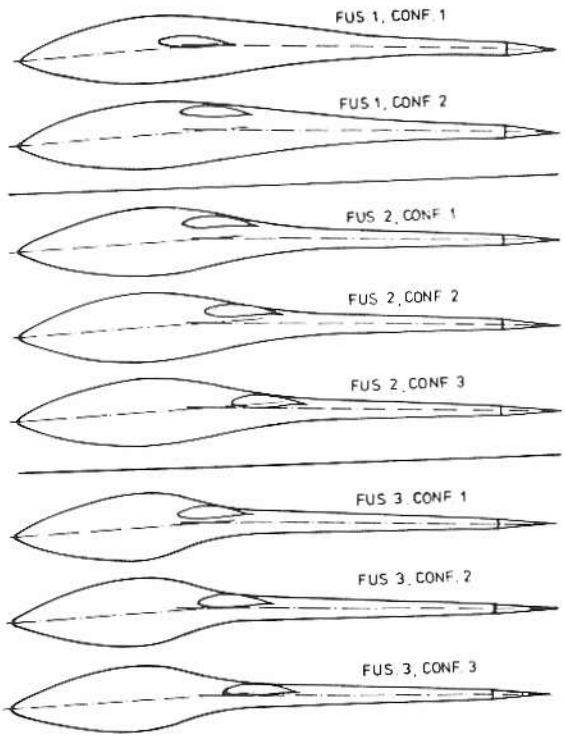

Fig. 1: Wing-fuselage combinations

The wing is untapered and has the airfoil FX62-K-131/17 (flap angle zero degrees). According to Ref. 2 a high wing position is preferable for aerodynamic reasons. Therefore, the wing on

the basic fuselage was shifted to a higher position than on the sailplanes mentioned before, resulting in fuselage 1, configuration 2. Similar wing positions are applied on fuselages 2 and 3, configuration 1. Configurations 2 and 3 are obtained by shifting the wing in two steps of 1/3 chord length backward.

Finally, fuselage 1 is provided with a mid-wing positioned 1/3 of the chord length forward in view of a two seat application.

In all cases, the wing is set at 1 degree incidence with respect to the tailboom axis.

Fuselage coordinates, position of wing leading edge and relevant data are given in Tables 1 to 3 and Fig. 2.

Fig. 3, deduced from measurements in Ref. 1, illustrates the effect of contraction ratio and wing location on the pressure distribution along the top and the underside of the fuselage.

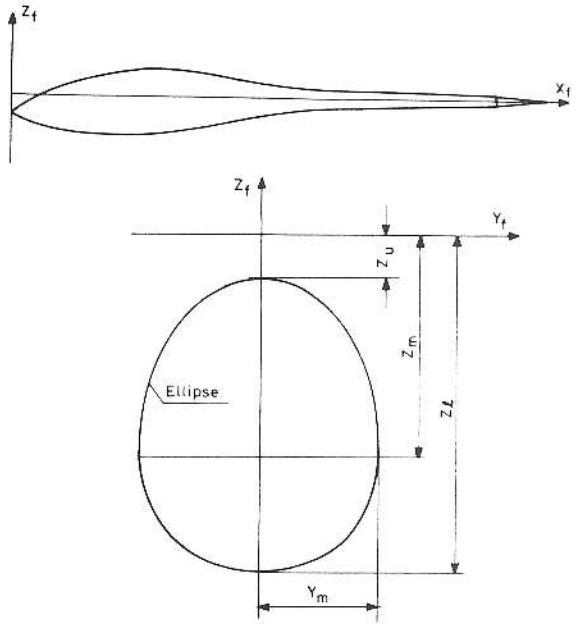

Fig. 2: Geometric definitions of table 1 and 2.

X_f	Fuselage 1				Fuselage 2				Fuselage 3			
	Y_m	Z_u	Z_m	Z_l	Y_m	Z_u	Z_m	Z_l	Y_m	Z_u	Z_m	Z_l
0	0	- 53	- 53	- 53	0	- 53	- 53	- 53	0	- 53	-53	- 53
60	30	- 12	- 58	- 82	30	- 12	- 58	- 82	30	- 12	- 58	- 82
120	47	20	- 60	-102	47	20	- 60	-102	47	20	- 60	-102
220	71	60	- 62	-126	71	60	- 62	-126	71	60	- 62	-126
320	89	90	- 61	-142	89	90	- 61	-142	89	90	- 61	-142
420	102	111	- 59	-152	102	111	- 59	-152	102	111	- 59	-152
520	107	121	- 57	-153	107	121	- 56	-152	107	121	- 52	-148
620	106	121	- 51	-146	105	119	- 50	-144	105	117	- 38	-125
720	101	115	- 45	-135	96	109	- 43	-129	87	94	- 23	- 96
820	94	107	- 37	-120	80	93	- 32	-109	61	68	- 10	- 67
920	85	97	- 28	-106	65	75	- 20	- 87	47	50	- 2	- 50
1020	75	87	- 19	- 92	51	58	- 9	- 61	45	45	0	- 45
1120	67	77	- 11	- 80	45	46	0	- 47	42	42	0	- 42
1220	60	67	- 4	- 68	39	39	0	- 39	39	39	0	- 39
1320	54	58	- 1	- 59	36	36	0	- 36	36	36	0	- 36
1420	50	51	0	- 51	33	33	0	- 33	33	33	0	- 33
2000	29	29	0	- 29	19	19	0	- 19	19	19	0	- 19
2200	0	0	0	0	0	0	0	0	0	0	0	0

Table 1: Coordinates of the fuselages (mm)

	X_f	Z_f
Fus. 1, Conf. 1	565	5
1 2	665	72
2 1	665	65
2 2	765	46
2 3	865	28
3 1	665	40
3 2	765	24
3 3	865	18

Table 2: Position of wing leading edge (mm)

	Frontal area (m^2)	Surface area (m^2)
Fus. 1	0.0461	0.965
2	0.0461	0.786
3	0.0461	0.731

Table 3: Fuselage data.

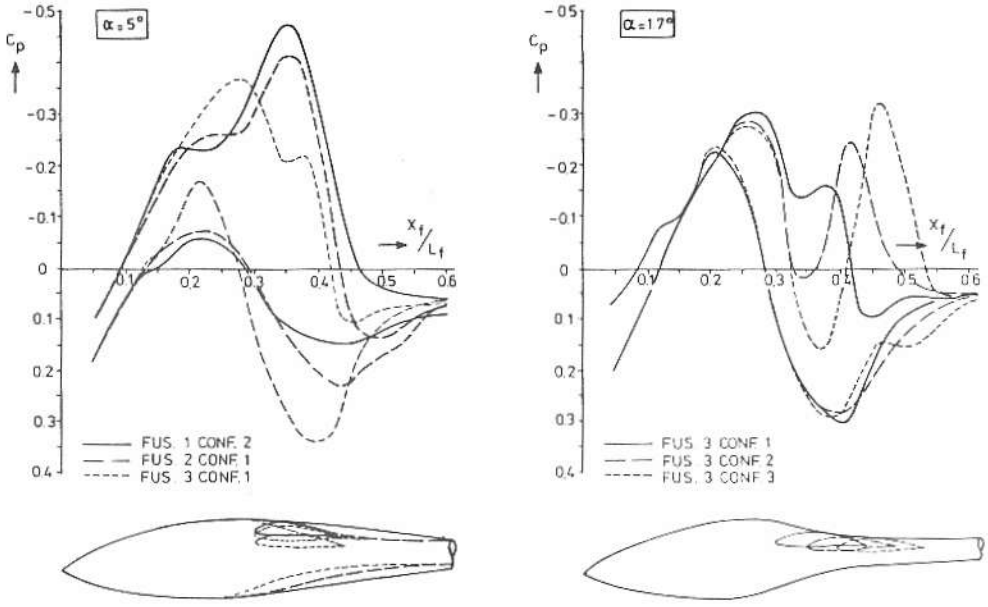

Fig. 3: Pressure distributions along the top and the underside of the fuselage, effect of contraction ratio and wing location.

WIND TUNNEL, MODEL SUPPORT AND TEST EQUIPMENT

The low-speed low-turbulence wind tunnel is of the closed return type and has an interchangeable octagonal test section 1.80 m wide and 1.25 m high. The turbulence level during the tests was of the order of 0.04%.

The models were mounted upside down as shown in Fig. 4. The axis of rotation, located at 40% chord, passed through the tunnel walls and was attached to a frame. This frame was suspended to the six component balance system of the wind tunnel. The gap between the wing tips, axis of rotation and wind tunnel walls was about 1 mm.

In addition to balance measurements of the isolated wing, drag measurements were performed with a wake rake traversing in spanwise direction at a distance of 20% chord downstream of the trailing edge. The rake utilized 15 total pressure tubes equally spaced at 2.5 mm, and 2 static pressure tubes. All pressures were recorded by an automatically reading multi-tube liquid manometer. Transition of the boundary layer was detected by a stethoscope. For flow visualization, the oil film technique was used.

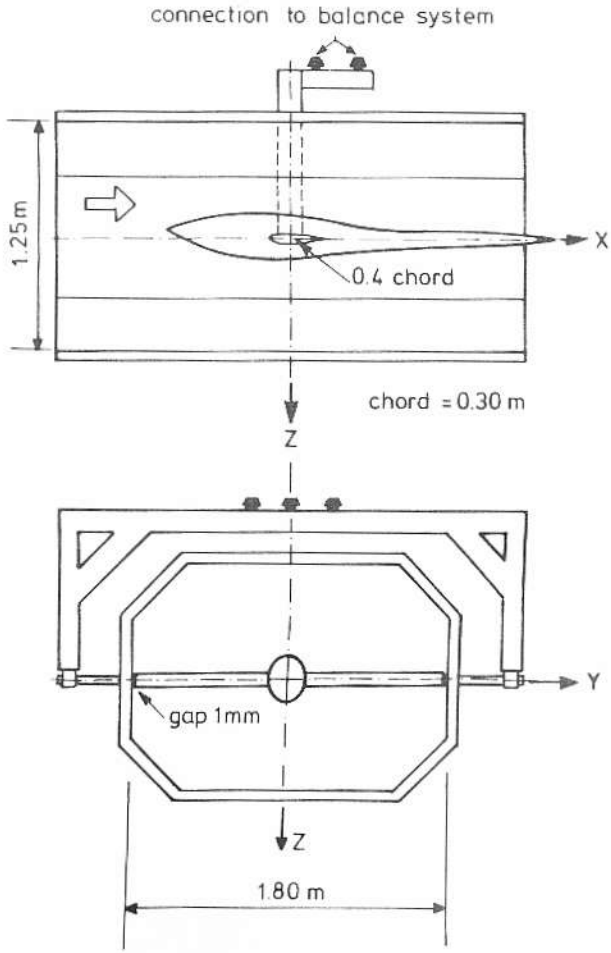

Fig. 4: Test set-up.

TESTS

The characteristics of the wing and wing-fuselage combinations were measured at a Reynolds number related to the wing chord of $1.23 * 10^6$. Some measurements were also performed at $Re_c = 0.7 * 10^6$. However, the results, being similar to the former ones, are not presented here.

At several wing-fuselage combinations tests were performed with roughness on the fuselage nose and with simulation of a canopy - both a short and a long canopy - which was not flush with the fuselage surface.

Oil flow patterns and stethoscope measurements were made to study the flow behavior on the combinations. In addition, to study the flow behavior in the junction region, oil flow patterns were made with a wing mounted on a reflection plate.

DATA REDUCTION

All balance and wake rake data were on line reduced and the lift, drag and moment characteristics, denoted by C_Z, C_X and C_M respectively, were plotted using the HP21MX-E computer of the Low Speed Laboratory.

Standard low-speed wind tunnel wall corrections, composed of solid and wake blockage, lift interference and wake-buoyancy, were applied according to Ref. 3 and 4. These corrections on the coefficients amount to 2% for the isolated wing and 5% for the wing-fuselage combinations. The correction on the angle of attack, being less than 0.1 degree was neglected.

The drag due to wing-tip, tunnel-wall interference was derived from balance and wake rake measurements of the isolated wing, Fig. 5. The wake rake was set at a spanwise position where the drag was equal to the mean of the drag distribution measured along 1.65 m span at three angles of attack within the low drag region ($\alpha = -1.5^0$, 0^0 and 5^0). In this region the drag difference between wake rake and balance measurements, plotted against the lift coefficient squared, is linear as shown in Fig. 6, indicating an effective aspect ratio of 115.

Beyond the low drag range the position of transition strongly depends on local airfoil shape quality, and a relatively high local drag coefficient may result as shown by the wake rake measurements. Similar results with the same linear

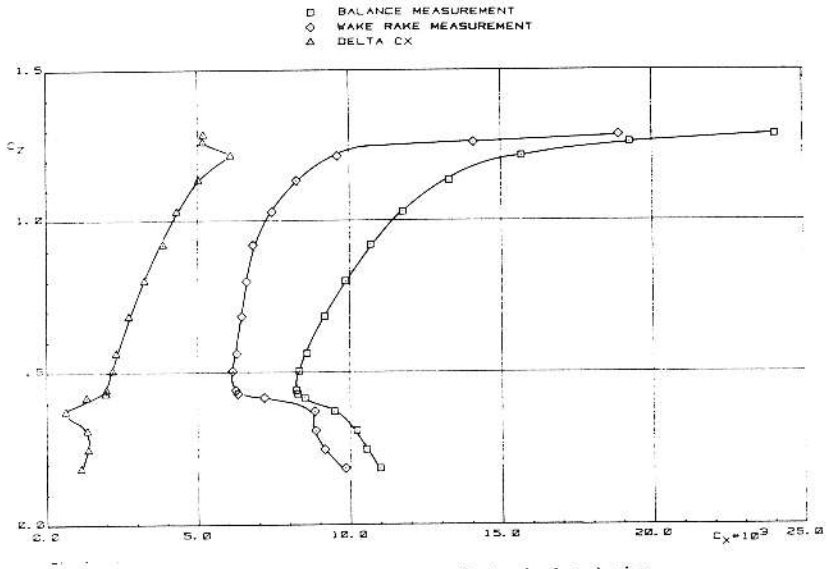

Fig. 5: Balance and wake rake measurements of the isolated wing

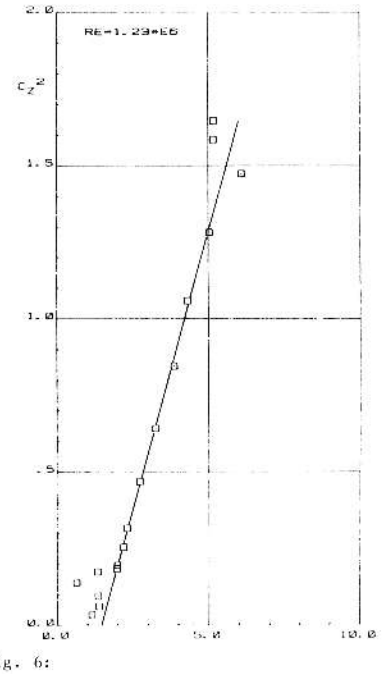

Fig. 6:

Drag difference between balance and wake rake measurements of the isolated wing against the lift coefficient squared

relationship were obtained at $Re = 0.7 * 10^6$. Hence, all balance measurements were corrected for wing-tip, tunnel-wall interference by taking into account, at corresponding angle of attack, a drag value according to this straight line relationship. As an example, Fig. 7 shows the mean profile drag of the isolated wing and the drag characteristics of the basic fuselage 1, configuration 2. In addition, the lift and moment characteristics are given.

These coefficients, based on the model wing surface of 0.54 m^2 and model wing chord of 0.30 m, were used in analyzing the effects of fuselage shape and wing location with respect to the isolated wing characteristics, and the effects of disturbances on the fuselage forebody.

In actual situations these effects are smaller due to the larger reference wing area. Hence, for sailplane performance estimation, the results were converted to a wing area of 10 m^2 which is typical for a high performance 15 m span sailplane. Assuming this wing has the airfoil characteristics as measured for the isolated wing, Fig. 7 also shows the characteristics converted to 10 m^2.

RESULTS

1. Wing-fuselage Interference Effects

To provide insight in the experimental results and related wing-fuselage interference effects, a description of the four main aerodynamic effects will be given, as compiled from Refs. 5 to 12.

a. Displacement Effects.
Due to the displacement of the fuselage the streamwise velocity distribution on the wing changes towards the junction, depending on the relative dimensions of the fuselage and wing and resulting curvature of the intersection lines. For instance, the velocity in the junction of a symmetrical wing, attached in a midwing position to a cylindrical fuselage, both set at zero angle of attack, is reduced except near the leading and trailing edges. Since the velocity distributions on upper and lower surface are equal, no lift results. If the ratio of wing thickness and fuselage diameter tends to zero, which represents the case of a wing attached to a reflection plate, the induced velocities vanish.

b. Effects of Asymmetry.
If the previous wing is shifted to a high-wing position, the intersection lines along the upper and lower surface differ. As a consequence, the velocities in the junction are decreased on the upper side and increased on the lower side. The lift curve is decreased by a more or less constant differential C_L. For a low-wing arrangement the opposite is true. Similarly, asymmetric displacement effects occur when the wing is cambered, or set at an angle to the fuselage, or shifted in longitudinal direction on a waisted fuselage.

c. Lift effects.
Consider again the cylindrical fuselage at zero angle of attack combined with a symmetrical wing in a mid-wing position, now set at an angle to the fuselage. Compared to the isolated wing, the interference reduces the spanwise and chordwise loadings towards the wing roots. The pressure distribution and circulation around the wing roots are transferred upon the fuselage in such a way that the loading decreases approximately elliptically between the junction and the axis.

When rotating the fuselage to the same angle of attack as the wing, there is a strong crossflow (named alpha flow) and hence an upwash along the sides of the fuselage which increases the lift curve slope. For instance, in the case of a circular cylindrical fuselage the angle of attack at the wing roots is doubled (because the velocity component which crosses the cylinder is doubled at the sides). Hence, the spanwise lift distribution shows peaks at the wing roots, and the wing roots show suction peaks at the leading edge. Again, if the wing is not in the midwing position, effects of asymmetry are introduced. For instance, if the fuselage has the same angle of attack as the wing, the lift at the wing roots decreases when the wing is shifted to a high (or low)

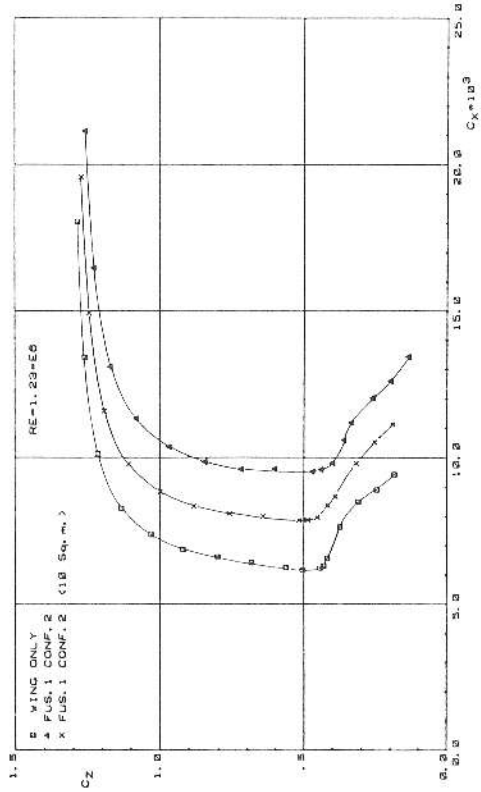

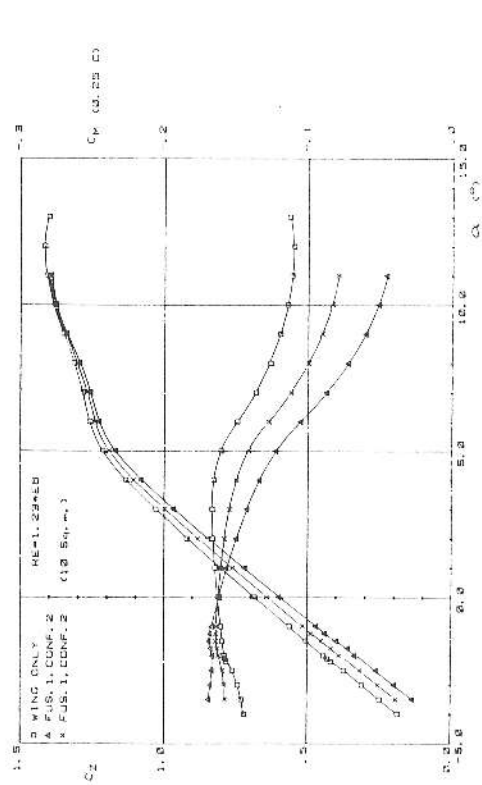

Fig. 7: Characteristics of the isolated wing, and of fuselage 1 configuration 2 based on the model wing area of 0.54 m^2 and converted to a wing area of 10 m^2

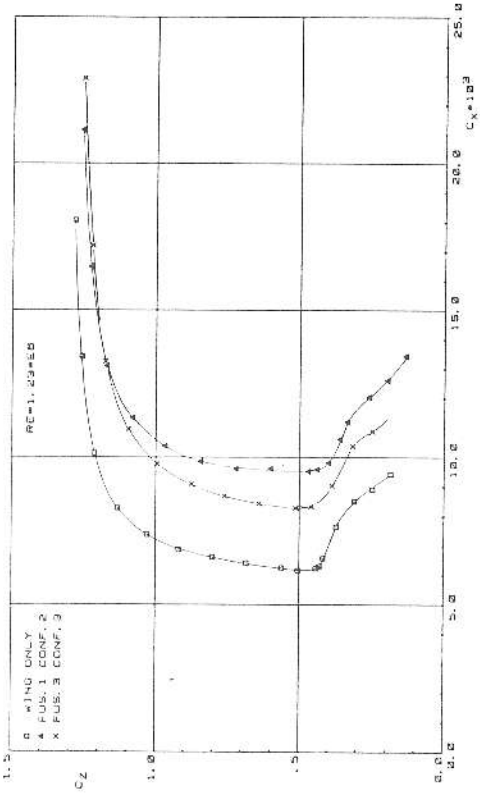

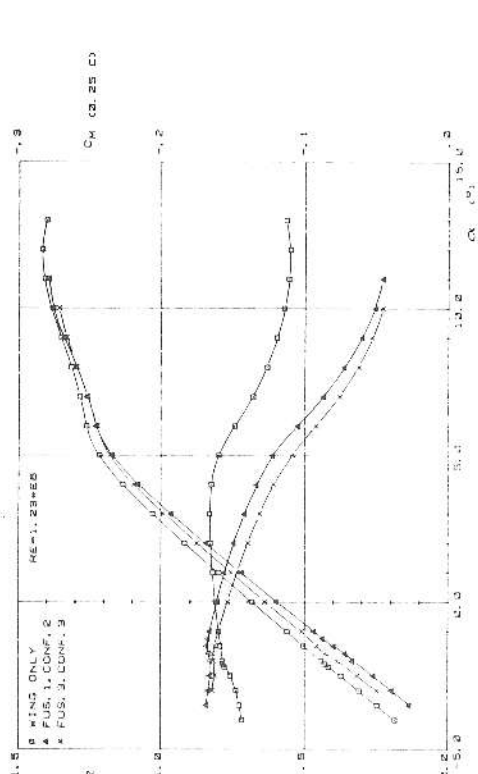

Fig. 8: Characteristics of the isolated wing and of two combinations, based on the model wing area

wing position due to the decrease of the angle of attack induced by the fuselage.

d. Effects of Viscosity.
The boundary layer on the fuselage is not able to overcome the adverse pressure gradient in front of the wing root leading edge and separates from the surface along a separation line at some distance around the junction. The separated surface rolls up into a vortex wrapped around the wing root (and, as will be shown, a second vortex is present closer to the junction). This viscous interference affects the lift at the junction in the same order as the previously described inviscid interference effects, but the influence extends far less in spanwise direction.

At higher angles of attack the flow separates at the rear part of the junction, affected by the induced angle of attack and the shape of the junction. These separated areas increase with angle of attack and a pair of vortices appear leaving the wing upper surface.

While there is extensive literature on wing-fuselage interference, relatively little has been published about the induced drag of wing-fuselage combinations. A difficulty in modern theories is that it is not known how the Kutta condition should be fulfilled. From classical theory, Ref. 12, the relation

$$C_{D_{i_{wf}}} = C_{D_{i_{ell.}}} \left(\frac{1}{1 - \left(\frac{d}{b}\right)^2} \right)^2$$

b = span

d = fuselage diameter

indicates an induced drag increment of only 0.5% for a 15 m span mid-wing configuration with a fuselage of 0.75 m diameter. A low additional induced drag is also obtained with the practical estimation procedure given in Ref. 5. However, at high lift coefficients flow separation in the junction affects the lift distribution and consequently the induced drag. In the next analysis of the experimental results the induced drag contribution is left out of the discussion.

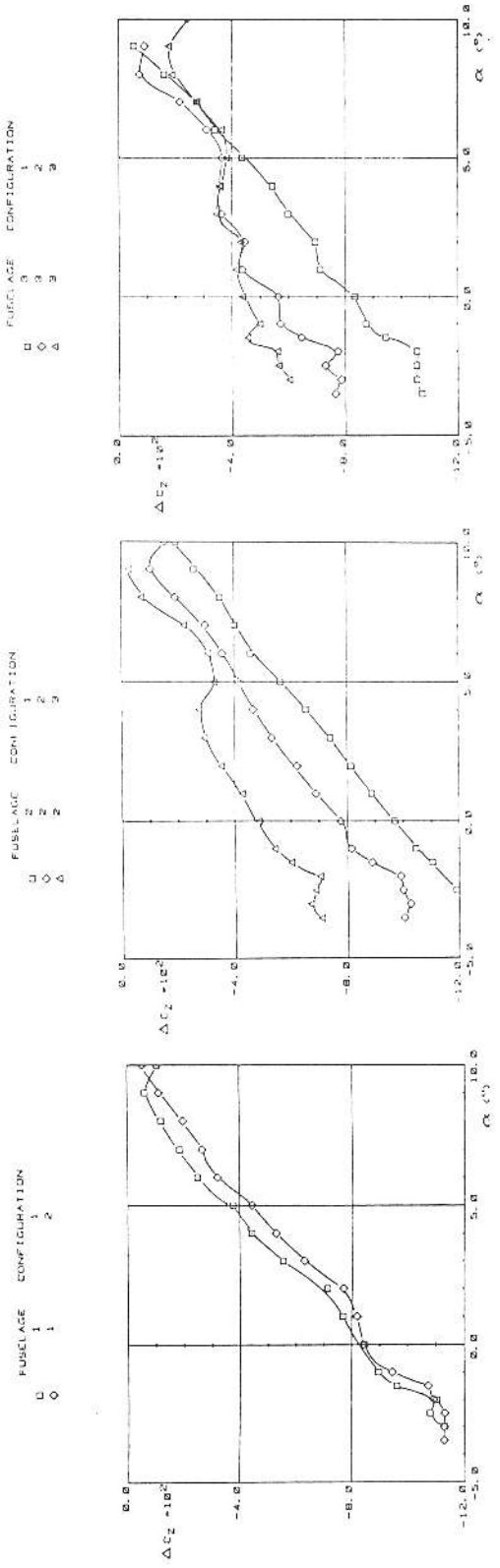

Fig. 9a: Lift differences with respect to the isolated wing, based on model wing area

2. Experimental Results

Now to the experimental results: Fig. 8 gives an indication of the largest

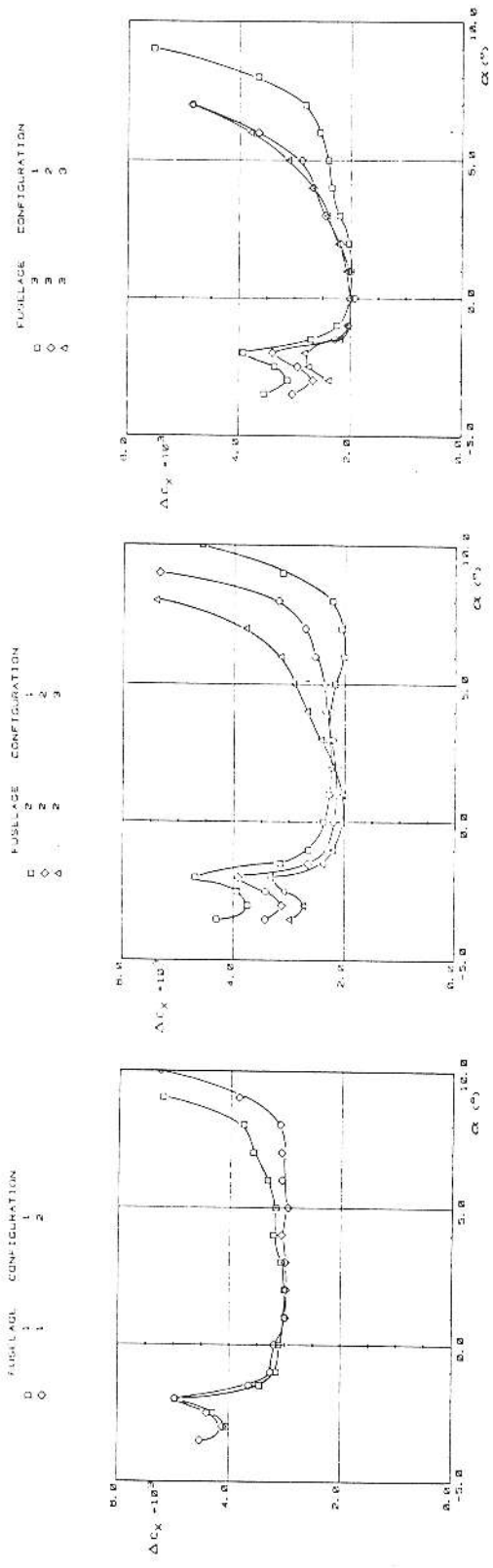

Fig. 9b: Drag differences with respect to the isolated wing, based on model wing area

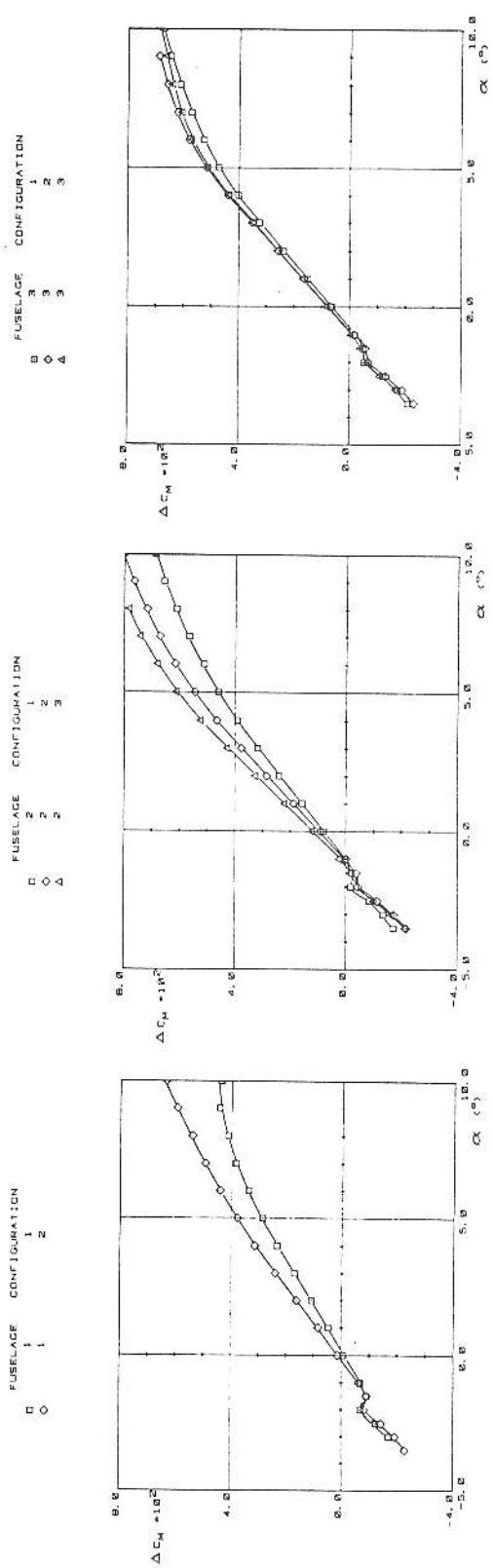

Fig. 9c: Moment differences with respect to the isolated wing, based on model wing area

differences in characteristics measured. Instead of showing the characteristics of all the combinations, the differences with respect to the isolated wing characteristics - being more suitable for comparison and analysis - are presented in Fig. 9.

The lift of the combination is generally lower than the lift of the isolated wing because the fuselage and interference generates less lift than the portion of the wing covered by the fuselage. If this portion decreases by shifting the wing upwards or backwards, or because of a higher fuselage contraction ratio, the lift decrement decreases.

The lift-curve slope of the combinations is generally higher than the lift-curve slope of the isolated wing due to alpha flow. However, for the most rearward wing location on fuselage 2 and for the intermediate wing location on fuselage 3, there is an extra loss of lift beyond about 3 degrees angle of attack. For the most rearward wing location on fuselage 3, this loss of lift starts at an even lower angle of attack. These combinations also show the highest drag increase with angle of attack. Obviously, the accumulation of boundary layer material coming from the forebody and flowing over the upper surface of the fuselage and junction, running up against the successive adverse pressure gradients of the fuselage contraction and the wing, leads to thick boundary layers and eventually early separation in the junction. (Separation at the trailing edge of the isolated wing starts at about 5 degrees angle of attack.) If the fuselage fits to the streamlines of the wing, cross-flow effects are minimized. (This design principle of streamline shaping was applied by Muttray in 1934, Ref. 11.) Hence, better results for fuselage 2, configuration 1 at 5 degrees angle of attack, in comparison to configuration 3, are largely due to better fitting of the forebody to the streamlines of the wing, as shown in Fig. 10.

Another effect due to alpha flow is the drag increase around -2 degrees angle of attack for all combinations. At this angle the drag of the isolated wing is low and at the lower boundary of the low drag bucket. On the combinations, however, the wing root areas are effectively at a more negative angle of attack, thus operating below the low drag bucket and causing the drag increase. At -3 degrees angle of attack the complete wing has turbulent flow on the lower surface as on the isolated wing, and the drag difference is smaller again. The drag increase of the combinations with fuselage 2 or 3 is at best 2/3 of the drag increase with fuselage 1. Since fuselage drag is mainly due to skin friction, the reduction in wetted surface for the waisted fuselages is primarily responsible for this drag reduction.

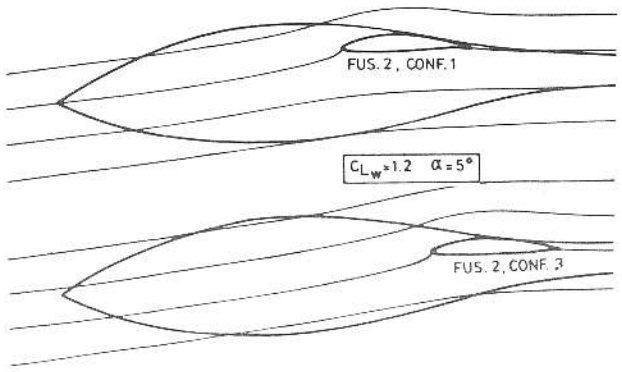

Fig. 10: Fuselage shape and streamlines of the wing flow

Finally, the differences in pitching moment coefficient about the quarter chord line show the destabilizing effect when a fuselage is added to the wing. This effect increases with angle of attack and with the length of the forebody.

In order to evaluate the effects of the various combinations on sailplane performance, the results were converted to a standard wing area of 10 m^2, and compared at equal values of the lift coefficient (i.e. flight speed). Similar to Fig. 8, an indication of the largest differences is given in Fig. 11. And similar to the previous analysis, differences in drag characteristics are presented, now with respect to the worst combination of fuselage 1, configuration 2.

The results, obtained by interpolation and plotted on a large scale in Fig. 12, show no practical drag difference for the two wing locations on fuselage 1. A significant and almost equal reduction has been obtained with the waisted fuselages 2 and 3. A rearward wing location has an advantage at the lower lift coefficients, but a disadvantage at high lift coefficients for reasons described before. Fuselage 2, configu-

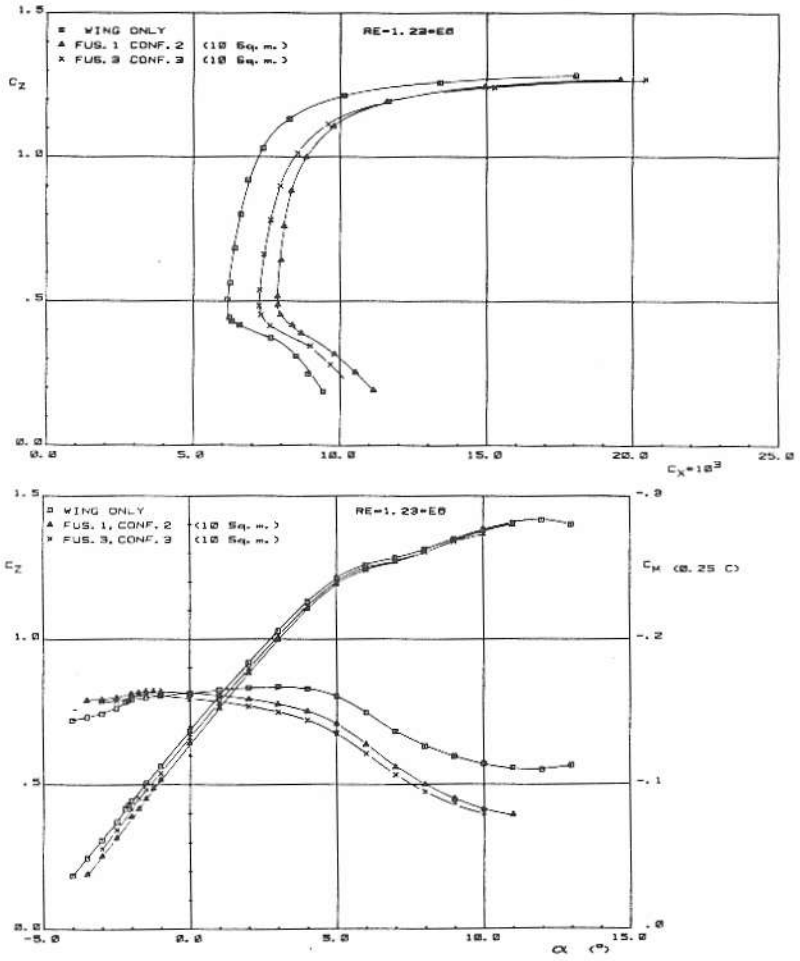

Fig. 11: Characteristics of the isolated wing and of two combinations, based on a wing area of 10 m^2

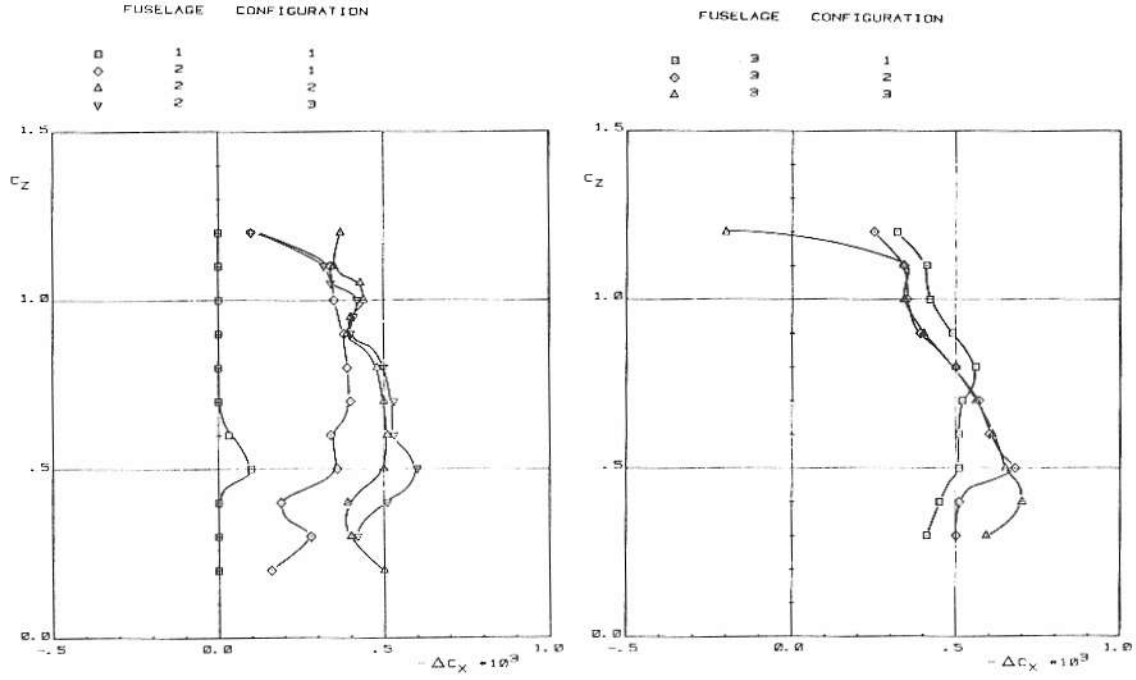

Fig. 12: Drag differences with respect to fuselage 1 configuration 2, based on a wing area of 10 m^2

ration 2 is aerodynamically equal to fuselage 3, configuration 1. As always, other aspects (as for instance the structural and aerodynamic consequences of negative wing sweep for center of gravity reasons) have to be considered as well in choosing the proper combination.

3. Flow Phenomena

The laminar boundary layer on the forebody of the fuselage is not able to run up far against the adverse pressure gradient caused by the contraction and induced in front of the wing root, and turns turbulent as shown in the flow pattern of Fig. 13. In the case of the rearward wing locations on fuselage 3, where both adverse pressure gradients are separated, the steep pressure gradient due to contraction causes a laminar separation bubble surrounding the fuselage. Occasionally, a grain in the oil substance caused a turbulent wedge as shown in Fig. 14. The large increase in turbulent area demonstrates the detrimental effect of disturbing the forebody flow.

The curved transition line on the wing upper surface in Fig. 15, interrupted by turbulent wedges again, indicates the effect of alpha flow. Turbulent separation occurs in front of the wing trailing edge and the rotating accumulation of oil in the junction fed from the separated trailing edge, Fig. 16, shows the origin of the vortices.

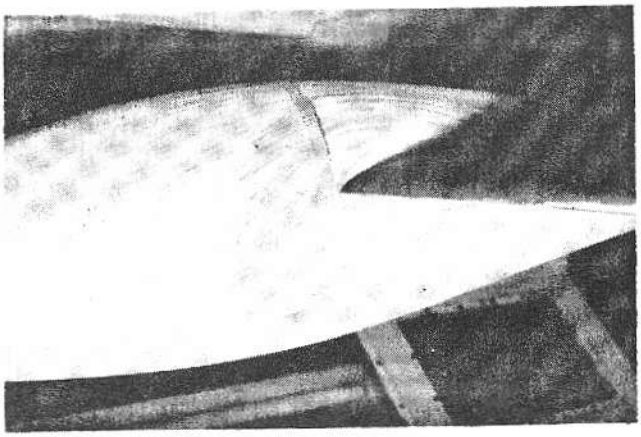

Fig. 13: Transition on the fuselage forebody

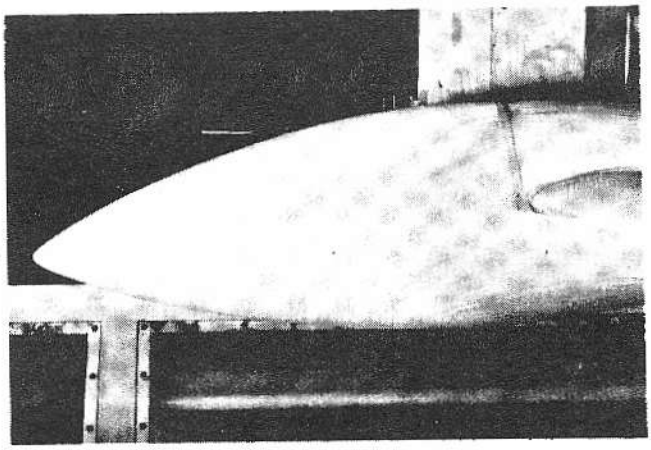

Fig. 14: Turbulent wedge on the fuselage forebody

$\alpha = 6^{o}$
$Re_c = 1.23 * 10^6$

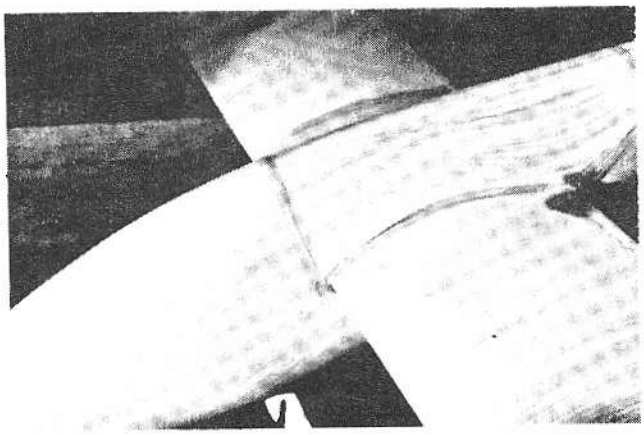

Fig. 15: Transition, turbulent wedges, and separation on the wing

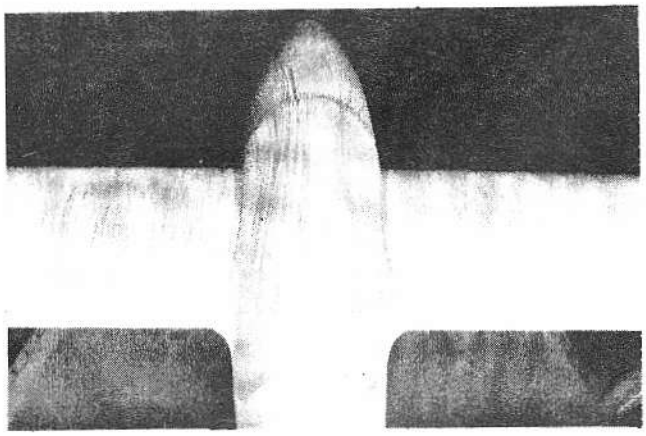

Fig. 16: Trailing edge separation and the origin of vortex

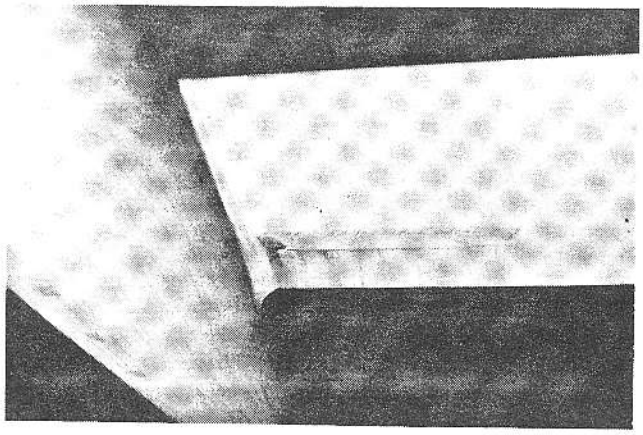

Fig. 17: Laminar separation bubble on lower wing surface

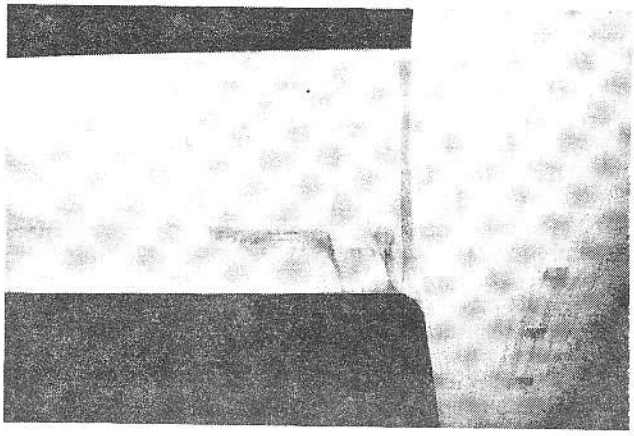

Fig. 18: Persistency of the laminar separation bubble between the turbulent wedges and the corner flow

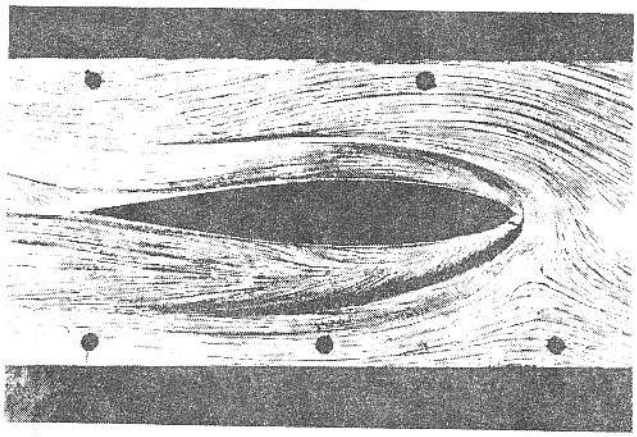

Fig. 19: Flow pattern on the reflection plate; $\alpha = 10^{o}$ $Re_c = 0.8 * 10^6$

On the lower surface, laminar flow followed by a laminar separation bubble, is present up to the junction flow, Fig. 17. The persistency of the bubble, illustrated by its presence between the turbulent wedges and the corner flow in Fig. 18, was noticed before in an experiment where air was blown through small orifices in a wing, periodically spaced in spanwise direction, to eliminate the laminar separation bubble, Ref. 13.

A complicated flow pattern was observed on the fuselage around the wing root, and a similar pattern was found on the tunnel wall around the wing tip when the gap was sealed. In order to eliminate the effect of gravity on the oil streaklines - there was some doubt about this effect - a more detailed flow investigation was performed with a rectangular wing with aspect ratio 7.5 and wing section NACA 64_2-A015, mounted vertically on a large reflection plate near the ceiling of the test section. The boundary layer on the plate was turbulent due to a transition strip near the leading edge. Fig. 19 shows a flow pattern made at 10 degrees angle of attack and a Reynolds number of $0.8 * 10^6$. The picture, taken after the wing was removed, clearly shows the dividing streamline in front of the airfoil which ends in a singular point on the separation line. According to Ref. 7 the separated surface rolls up into a vortex wrapped around the wing root. As shown in the picture, a second vortex is present closer to the junction, which merges with the first one on the upper surface. A separated region behind about 50% chord upper surface is clearly marked.

4. Disturbance of the Forebody Flow

In order to measure the drag penalty due to distrubances on the fuselage and to verify a method to calculate the critical roughness height, several combinations were provided with artificial roughness on the forebody. Fig. 20 shows results for different types of roughness at 5% of the fuselage length. Fully turbulent flow and equal drag coefficients were obtained with a tape of 2.25 mm thickness with digged-in

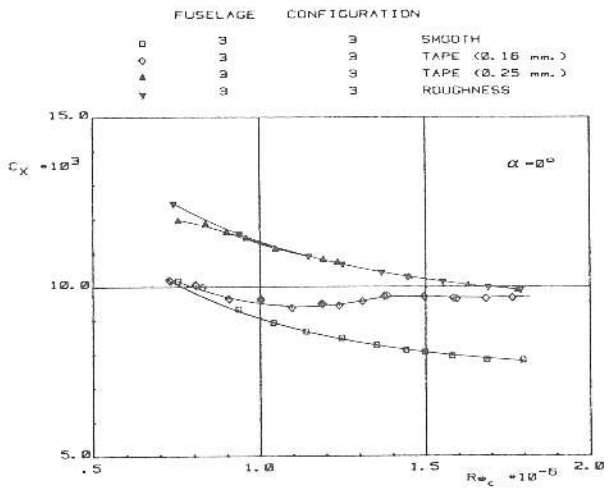

Fig. 20: Drag penalty due to different types of roughness on the fuselage nose (5% fuselage lenght) based on model wing area

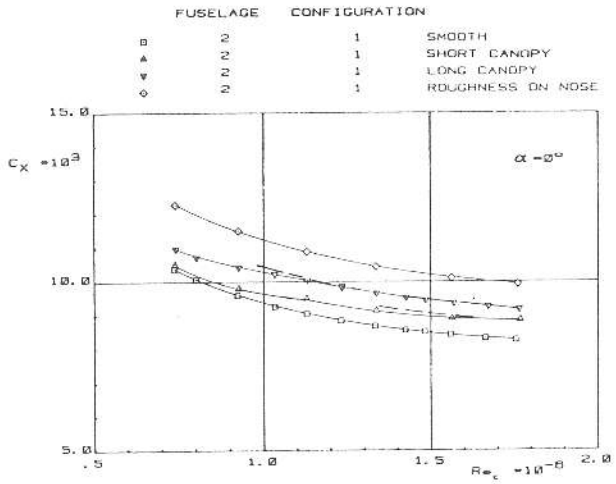

Fig. 22: Drag penalty due to a protruding canopy front edge (step height 0.25 mm on scale) and complete turbulent fuselage flow, based on model wing area

bumps of 1 mm height every 5 mm, or with a row of squares of tape with the same thickness and measuring 5 mm on the sides. The results are simply denoted by "roughness." A 0.16 mm thick flat tape starts to be effective at $Re_c = 0.7 * 10^6$, and is fully effective near $Re_c = 2 * 10^6$. Similarly, a 0.25 mm thick tape is fully effective at about $Re_c = 1 * 10^6$.

These results are in fair agreement with calculations according to the method of Ref. 14 if the proper roughness Reynolds numbers are applied, Fig. 21. In the left part of this figure, the maximum height of roughness which can be accepted as having no effect upon the drag is shown; the roughness Reynolds number is applicable in case of two dimensional excrescences as shown in Ref. 15. Similarly, the right part of the figure shows the minimum height of roughness which guarantees transition without adding undue extra drag due to it; the roughness Reynolds number is valid for roughness bands. (A slightly lower value, $/R_k = 24.5$, is relevant in calculating the permissible - not disturbing - height of isolated excrescences). The figures indicate that in actual practice (scale factor 1:3) the flow will be laminar up to high flight speed ($Re_c = 3 * 10^6$) when the roughness height is below a few tenths of a millimeter.

A canopy front edge which protrudes from the fuselage surface, producing a step of 0.75 mm height, was simulated by sticking 0.25 mm thick tape to the surface. Both a long and a short canopy were simulated, Fig. 24. The results, as illustrated in Figs. 22 and 23, show a drag increase which is roughly proportional to the increase in turbulent area, and independent of the angle of attack. The Reynolds numbers at which the step starts to produce turbulent flow or is fully effective, are in fair agreement with the calculations again. In conclusion, if flow disturbance by the canopy front edge is unavoidable, the short canopy is preferable because the edge is closer to the natural transition position of the smooth fuselage and in an area where the laminar boundary layer is less sensitive to roughness than in the nose region. Finally, Fig. 24 shows the drag values for the three different fuselages and equal wing position, coverted to 10 m^2, indicating the trend of the drag and drag increase due to a (fully) distrubing canopy front edge or complete turbulent fuselage flow.

CONCLUDING REMARKS

Some general qualitative conclusions, useful in designing a wing-fuselage combination for a high performance sailplane, are summarized.

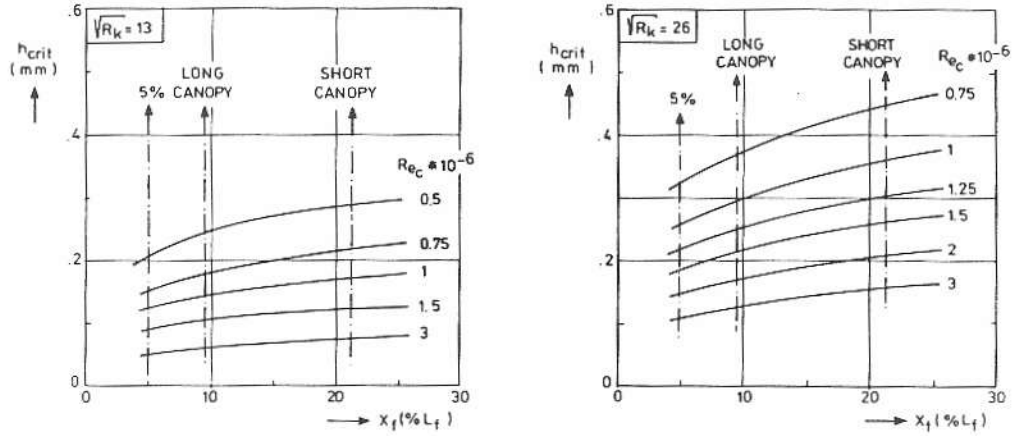

maximum roughness height which is ineffective (two dimensional)

minimum roughness height which is fully effective

Fig. 21: Calculated critical roughness heights

To minimize crossflow effects and postpone separation in the rear part of the junction, the fuselage shape should be fitted to the streamlines of the wing produced at a relatively high lift coefficient. The pressure gradients along the top of the fuselage due to contraction and due to the wing may be combined with each other to postpone transition. On the fuselage, underside contraction should start behind the pilot's seat but not later than the (disturbing) wheel doors. The effects of contraction ratio and wing location have been shown in this paper.

The flow in the junction is anything but laminar. Hence, great care has to be taken when those laminar wing airfoils are applied which have separation problems in case of turbulent flow conditions. As shown in Ref. 16, several well-known airfoils have these problems when the leading edge is contaminated by insects or wetted by rain. By properly modifying the airfoil towards the junction, or by applying wing-fuselage fairings (thus manipulating the pressure gradients and load distribution by airfoil extension), these problems can be alleviated. In addition, a properly shaped leading edge fairing eliminates the local stagnation region and, hence, suppresses the formation of the vortices around the junction, as shown in Refs. 17 and 18.

In designing wing-fuselage combinations and fairings, basic potential flow information, obtained from a three-dimensional panel method, is indispensible. As in airfoil design, an inverse method such as the panel-like method of Ref. 19, developed for the design of a wing with prescribed pressure distribution and geometric constraints in the presence of a fuselage, is of great use. Application of these methods, together with experience as obtained in the present investigation, may lead to improved wing-fuselage combinations.

ACKNOWLEDGEMENT

The authors are grateful to the Staff of the DFVLR Institut fur Entwurfsaerodynamik for providing the wind tunnel models, and to Mr. J.J.H. Blom for preparing the airfoil streamline pattern computer program.

REFERENCES

1. Radespiel, R.: Experimentelle Untersuchungen an Segelflugzeugrumpfen mit verschiedener Einschnurung und Flugelanordnung. DFVLR Braunschweig, Institut fur Aerodynamik. In German, Unpublished students-thesis, 1979.

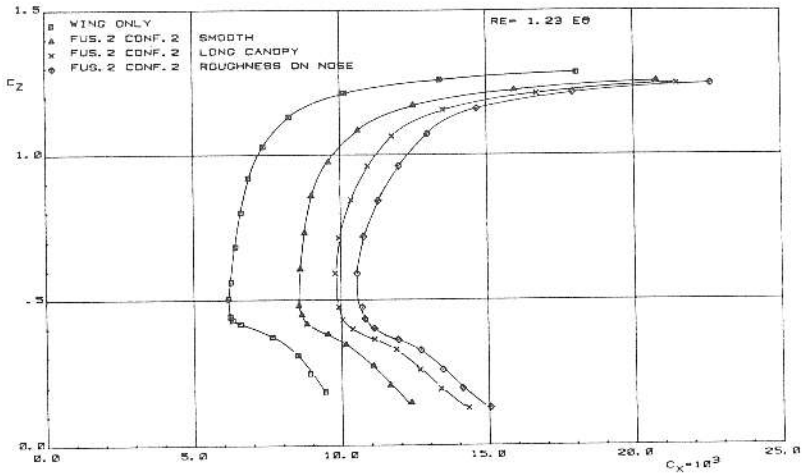

Fig. 23: Characteristics of fuselage 2 configuration 2 with disturbances on the fuselage forebody, based on model wing area

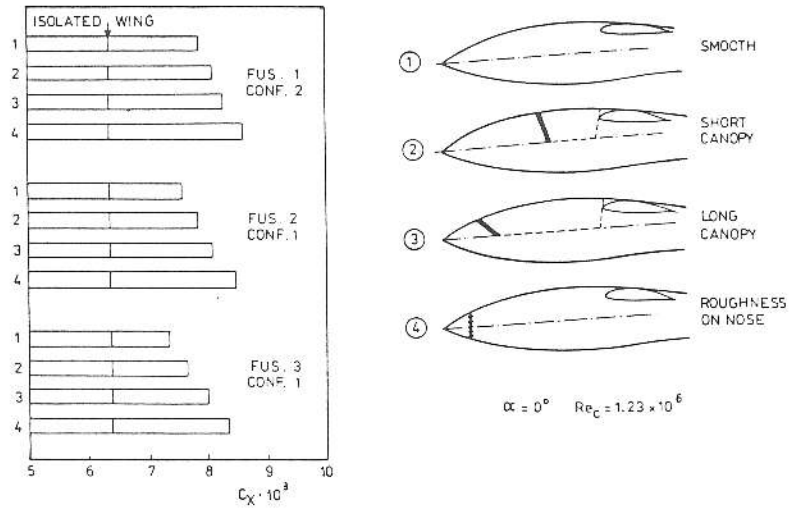

Fig. 24: Drag penalty due to disturbances on the forebody of the three fuselages with equal wing location, based on 10 m^2

2. Thomas, F.: Grundlagen fur den Entwurf von Segelflugzeugen. Motorbuch Verlag, Stuttgart, 1979.
3. Garner H.C.; Regers, E.W.E.; Acum, W.E.A.; Marshell, E.C.: Subsonic wind tunnel wall corrections. AGARDograph 109, 1966.
4. Allen, H.J.; Vincenti, W.G.: Wall interference in a two-dimensional flow wind tunnel, with consideration of the effect of compressibility. NACA Report no. 782, 1944.
5. Hoerner, S.F.: Fluid-Dynamic Drag. Published by the Author, Brick Town, 1965.
6. Hoerner, S.F.; Borst, H.V.: Fluid-Dynamic Lift. Published by the Author, Brick Town, 1975.
7. Kuchemann, D.: The aerodynamic design of aircraft. Pergamon Press, 1978.
8. Korner H.: Berechnung der potentialtheoretischen Stromung um Flugel-Rumpf-Kombinationen und Vergleich mit Messungen. Zeitschrift fur Flugwissenschaften 20, Heft 9, 1972.
9. Althaus, D.: Windtunnel measurements on bodies and wing-body combinations. Motorless Flight Research, NASA CR 2315, 1972.

10. Jacobs, E.N.; Ward, K.E.: Interference of wing and fuselage from tests of 209 combinations in the NACA variable density tunnel. NACA Report 540, 1935.
11. Muttray, H.: Die aerodynamische Zusammenfugung von Tragflugel und Rumpf. Luftfahrtforschung 11, 1934.
12. Durand, W.F.: Aerodynamic Theory, vol. IV. Julius Springer Verlag, 1935.
13. Boermans, L.M.M.; Oolbekkink, B.: Windtunnel tests on an outer wing segment of the ASW-19X sailplane. Report LR-369, Delft University of Technology, Dept. of Aerospace Eng., 1983.
14. Braslow, A.L.; Know, E.C.: Simplified method for determination of critical height of distributed roughness particles for boundary layer transition at Mach numbers from 0 to 5. NACA Technical Note 4363, 1958.
15. Young, A.D.; Paterson, J.H.: Aircraft Excrescence Drag. AGARDograph 264, 1981.
16. Boermans, L.M.M.; Selen, H.J.W.: Design and tests of airfoils for sailplanes with an application to the ASW-19B. ICAS-82-5.5.2, 1982.
17. Jupp, J.A.: Interference aspects of the A310 high speed wing configuration. Paper 11, AGARD CP no. 285, Subsonic/Transonic Configuration Aerodynamics, 1980.
18. Rubbert, P.E.; Saaris, G.R.: Review and evaluation of a three dimensional lifting potential flow analysis method for arbitrary configurations. AIAA Paper 72-188, 1972.
19. Fray, J.M.J.; Sloof, J.W.: A constrained inverse method for the aerodynamic design of thick wings with given pressure distribution in subsonic flow. Paper 16, AGARD CP 285, Subsonic/Transonic Configuration Aerodynamic, 1980.